AGU PUBLICATIONS

JGR

Journal of Geophysical Research: Solid Earth

RESEARCH ARTICLE
10.1002/2016JB013698

Key Points:
- Network translations from surface mass transport models cannot account for the variability in SLR translations
- We identify colored noise in SLR translations, increasing uncertainties in the rates fivefold (upper bound) compared to white noise only
- When using a power law and white noise model the SLR *Z* rate uncertainty (±0.33 mm/yr; 1 sigma) is improved 27% since ITRF2008

Supporting Information:
- Supporting Information S1

Correspondence to:
A. R. Riddell,
anna.riddell@utas.edu.au

Citation:
Riddell, A. R., M. A. King, C. S. Watson, Y. Sun, R. E. M. Riva, and R. Rietbroek (2017), Uncertainty in geocenter estimates in the context of ITRF2014, *J. Geophys. Res. Solid Earth*, *122*, 4020–4032, doi:10.1002/2016JB013698.

Received 30 OCT 2016
Accepted 26 APR 2017
Accepted article online 28 APR 2017
Published online 13 MAY 2017

Uncertainty in geocenter estimates in the context of ITRF2014

Anna R. Riddell[1,2], Matt A. King[1], Christopher S. Watson[1], Yu Sun[3], Riccardo E. M. Riva[3], and Roelof Rietbroek[4]

[1]Surveying and Spatial Sciences, School of Land and Food, University of Tasmania, Hobart, Tasmania, Australia, [2]Geoscience Australia, Canberra, ACT, Australia, [3]Department of Geoscience and Remote Sensing, Delft University of Technology, Delft, Netherlands, [4]Institute of Geodesy and Geoinformation, University of Bonn, Bonn, Germany

Abstract Uncertainty in the geocenter position and its subsequent motion affects positioning estimates on the surface of the Earth and downstream products such as site velocities, particularly the vertical component. The current version of the International Terrestrial Reference Frame, ITRF2014, derives its origin as the long-term averaged center of mass as sensed by satellite laser ranging (SLR), and by definition, it adopts only linear motion of the origin with uncertainty determined using a white noise process. We compare weekly SLR translations relative to the ITRF2014 origin, with network translations estimated from station displacements from surface mass transport models. We find that the proportion of variance explained in SLR translations by the model-derived translations is on average less than 10%. Time-correlated noise and nonlinear rates, particularly evident in the *Y* and *Z* components of the SLR translations with respect to the ITRF2014 origin, are not fully replicated by the model-derived translations. This suggests that translation-related uncertainties are underestimated when a white noise model is adopted and that substantial systematic errors remain in the data defining the ITRF origin. When using a white noise model, we find uncertainties in the rate of SLR *X*, *Y*, and *Z* translations of ±0.03, ±0.03, and ±0.06, respectively, increasing to ±0.13, ±0.17, and ±0.33 (mm/yr, 1 sigma) when a power law and white noise model is adopted.

1. Introduction

The need to monitor global change processes, such as sea level change and postglacial rebound, at a level below 1 mm/yr, illustrates the requirement for an accurate and precise global geodetic reference frame. The International Terrestrial Reference Frame (ITRF) [*Altamimi et al.*, 2016] attempts to meet accuracy and stability goals of 1 mm and 0.1 mm/yr, respectively [*Gross et al.*, 2009]. As each iteration of the ITRF provides improvements in the precision and accuracy of the global reference frame, challenges remain to meet the accuracy and stability goals. Particularly challenging is the realization of the origin (defined as the long-term averaged center of mass (CM) of the Earth) and its evolution in time [*Dong et al.*, 2014]. Presently, this realization is limited given that it is determined using measurements from a single measurement technique (satellite laser ranging (SLR)) [*Altamimi et al.*, 2016; *Wu et al.*, 2011] that is known to be affected by systematic biases and network asymmetry [*Appleby et al.*, 2016]. The ITRF2014 (and each predecessor) is a linear frame by definition, and consequently, the long-term motion of its origin is described by a linear trend. Limitations arise given that when specifying the ITRF origin to coincide with the long-term origin of the SLR frame, only time-constant annual and semiannual terms are included with a white noise model [*Altamimi et al.*, 2007, 2011, 2016; *Argus*, 2012], neglecting any other nonlinear motions as part of the functional or stochastic model.

Relative motion between the center of mass of the total Earth system (CM) and the center of surface figure (CF) of the solid Earth can be observed using space geodetic observations that tie Earth-fixed permanent geodetic sites and space-based satellite platforms. Both secular and seasonal geocenter motion occur as a result of past and present mass redistribution, where geocenter motion is the difference between CM and CF (the difference between geophysically determined origins). Past mass redistribution on the surface or interior such as glacial isostatic adjustment (GIA) induces secular geocenter motion, while intra-annual, seasonal, and interannual signals relate to present-day distributions, such as exchanges within and between the ocean, atmosphere, continents, and cryosphere [*Argus*, 2012; *Dong et al.*, 1997; *Wu et al.*, 2012]. SLR translations with respect to the ITRF2014 origin therefore consist of both measurement error and a component of real geocenter motion affected by the nonhomogenous network distribution of SLR tracking stations. This leads to a

sampling bias known as the "network effect," and should ideally reflect the offset between the network origin (CN) and the CM rather than the geocenter motion.

An alternative approach to studying geocenter motion uses observations and numerical models of surface mass transport to derive deformation of the solid Earth at the locations of the SLR stations (that change over time), from which network translations may be estimated. The mass transport models provide bounds on the network translations which are to be expected from known surface loading processes. Any inconsistency between observed SLR translations and those derived from a surface loading model will hint at problems in either the SLR methods (observations or processing) or problems within the surface loading model. In this paper, SLR translations and output from two surface loading models are used to assess the uncertainty in the SLR translations with respect to the ITRF2014 long-term origin.

2. Data

The origin of ITRF2014 is defined such that there are zero translation parameters and rates at epoch 2010.0 between the International Laser Ranging Service (ILRS) long-term mean origin from SLR and ITRF2014 [*Altamimi et al*., 2016]. The SLR temporal translation components used here have been derived with respect to the ITRF2014 origin that has been defined using the internal constraint method described in *Altamimi et al.* [2007] and *Altamimi et al.* [2016]. The translations were estimated using a seven-parameter similarity transformation between each week and a SLR ITRF2014 network of 21 core stations. The time series of the seven parameters were adjusted globally, in one run using the CATREF software (Combination and Analysis of Terrestrial Reference Frames) [e.g., *Altamimi et al*., 2016], with the full variance-covariance information of the total SLR SINEX time series. We analyze the translations from weekly combined SLR solutions relative to the ITRF2014 (linear) origin over the time span 1993.0 to 2015.0 in the temporal and spectral domains. The complete ILRS SLR reference frame solutions in SINEX format submitted for the realization of ITRF2014 covers the time span 1983.0 to 2015.0. Only the data from 1993.0 onward are used here due to noisy data in the early section of the time series, producing large formal uncertainties in the SLR translation series before the LAGEOS-2 satellite was launched in 1992 [*Dong et al*., 2014]. We compare the SLR translation time series with respect to the ITRF2014 long-term origin with two different estimates of network translations that are derived from independent surface mass transport models.

The ITRF2014 origin is considered theoretically representative of the long-term CM, where geocenter motion is defined as motion of the CM with respect to the CF [*Altamimi et al*., 2016]. Linear motions for ground stations are assumed, with some discontinuities and postseismic deformations enforced for sites affected by major earthquakes or equipment changes. The ITRF origin reflects CM on secular timescales due to it coinciding with the long-term average CM as observed by SLR, but on shorter (including seasonal) timescales, the ITRF origin reflects CF [*Blewitt*, 2003; *Collilieux et al*., 2009; *Dong et al*., 2003]. We note that some of the literature considers the opposite convention, that is, displacement of CF with respect to CM [e.g., *Métivier et al*., 2010; *Dong et al*., 2014].

Our first comparative geophysical model is from *Rietbroek et al*. [2015], who calculated surface mass transport loading based on a combination of Gravity Recovery and Climate Experiment (GRACE) and radar altimetry data using an inversion approach that applied conservation of mass to solve the sea level equation [*Rietbroek et al*., 2016]. Surface displacement components are provided for the time span 2002.3 to 2014.5 with monthly sampling, hereon referred to as R15. R15 considers mass redistribution from the Antarctic and Greenland ice sheets, land glaciers, GIA, continental water storage, and contributions from the oceans and atmosphere. Although GRACE alone is not capable of observing degree-1 mass redistribution, combination with additional data sets and use of an inversion methodology enables derivation of surface mass transport values. The short data span is limiting given that it covers only half of the SLR series but remains useful given the independent GRACE-based approach.

Our second data set was estimated from numerical surface mass transport models and solves the sea level equation to conserve mass for the global system after taking into account self-attraction and loading effects [*Gordeev et al*., 1977; *Frederikse et al*., 2016; *Tamisiea et al*., 2010] using fingerprints [*Mitrovica et al*., 2001] to represent the nonuniform redistribution of water. Hereon, this modeled surface mass product is referred to as MSM. MSM yields values over the time span 1993.0 to 2015.0 with monthly sampling. This data set includes modeled ocean and atmosphere mass redistribution (defined using the

AOD1B product) [*Flechtner et al.*, 2015], continental land glaciers [*Marzeion et al*., 2015], Greenland [*van den Broeke et al*., 2016], and Antarctic ice sheet surface mass balance changes from the Regional Atmospheric Climate Model (RACMO) version 2.3 [*Noël et al*., 2015], Global Reservoir and Dam database (GRanD) dam water retention [*Lehner et al*., 2011] using the filling rate method of *Chao et al*. [2008], and other terrestrial water storage from the Noah Global Land Data Assimilation System (GLDAS) product [*Rodell et al*., 2004]. Both the land glacier and dam retention components are sampled annually and have been linearly interpolated to monthly intervals for consistency with the other data sets, constraining the temporal resolution. It would be expected for these components to contain annual signals due to the seasonal nature of hydrologic mass exchange, and we return to this in section 4. A groundwater component is available using data from *Wada et al.* [2010]. The contribution from groundwater to the overall signal is primarily linear with very small annual amplitude for the available period. Further data description for MSM is available in the supporting information (Text S1) and *Frederikse et al.* [2016], including uncertainties for the component contributions.

Surface displacements from each geophysical model were derived by redistributing loaded masses within a thin shell on the Earth's surface. They are spherically symmetric, stratified, and nonrotating Earth responses elastically redistributed over subsecular (subdaily to decadal) timescales. The displacements are proportional to the incremental load potential according to the load Love number theory [*Farrell*, 1972] and are derived from the preliminary reference Earth model elastic Earth model (PREM) [*Dziewonski and Anderson*, 1981].

Following the methodology of *Collilieux et al*. [2009], network translations have been derived from station displacements due to loading effects from two distinct surface mass transport models and compared with SLR translations with respect to the ITRF2014 long-term origin to account for the network effect of the SLR station geometry.

From each of the geophysical models, network translations are computed following the methodology of *Collilieux et al*. [2009], using the ITRF2014 station positions and velocities plus the modeled surface mass loading deformation at each epoch of the respective data set. At each epoch, we used only those SLR sites that were active. The monthly surface deformation values are interpolated from monthly to weekly values using a cubic spline. The two synthetic time series are then used to estimate transformation parameters, using Globk [*Herring et al*., 2015], with respect to ITRF2014 using the full covariance matrix of the ILRS combined solution submitted for ITRF2014 analysis. Following *Collilieux et al.* [2012], only three rotations and three translations were estimated (that is, scale was not estimated). Repeating the analysis with the scale parameter included produced only negligible changes to the estimated transformation parameters. Covariance information was used as given; an occasional site was automatically removed for a given week due to the estimated station adjustments being larger than 10 sigma. Given that the ILRS combined solution was generated using a loose constraint approach, correlations exist between the Helmert parameters where some of the station displacements may leak into the rotation parameters [*Collilieux et al*., 2009]. Here the rotations have a mean and standard deviation of 0.00±0.02 milliseconds of arc for all components from both models (1 sigma), which induces station displacements below 1 mm.

The two network translation models, R15 and MSM, are compared with the SLR translation components with respect to the ITRF2014 origin to assess the sensitivity of the SLR observed origin against geophysically modeled geocenter motion taking into account the network effect of the SLR observing network.

3. Comparison of SLR and Modeled Network Translations

By construction, there are zero translation rates (trends) between ITRF2014 and the SLR stacked frame of weekly solutions over the time span 1993.0 to 2015.0. Annual and semiannual periodic signals were not removed from the SLR translation components as these are signals of interest. Figures 1a–1c show the three data sets in the temporal domain sampled at monthly epochs for clarity. The surface deformation values at each site were detrended before transformation [*Collilieux et al*., 2009]. Formal errors are not available for either of the surface mass transport models, but uncertainties are available for the constituent data sets that contribute to each model. Further information on the model uncertainties can be found in the associated references. Our use of two geophysical models aims to reflect, at least partly, the uncertainty in the two models.

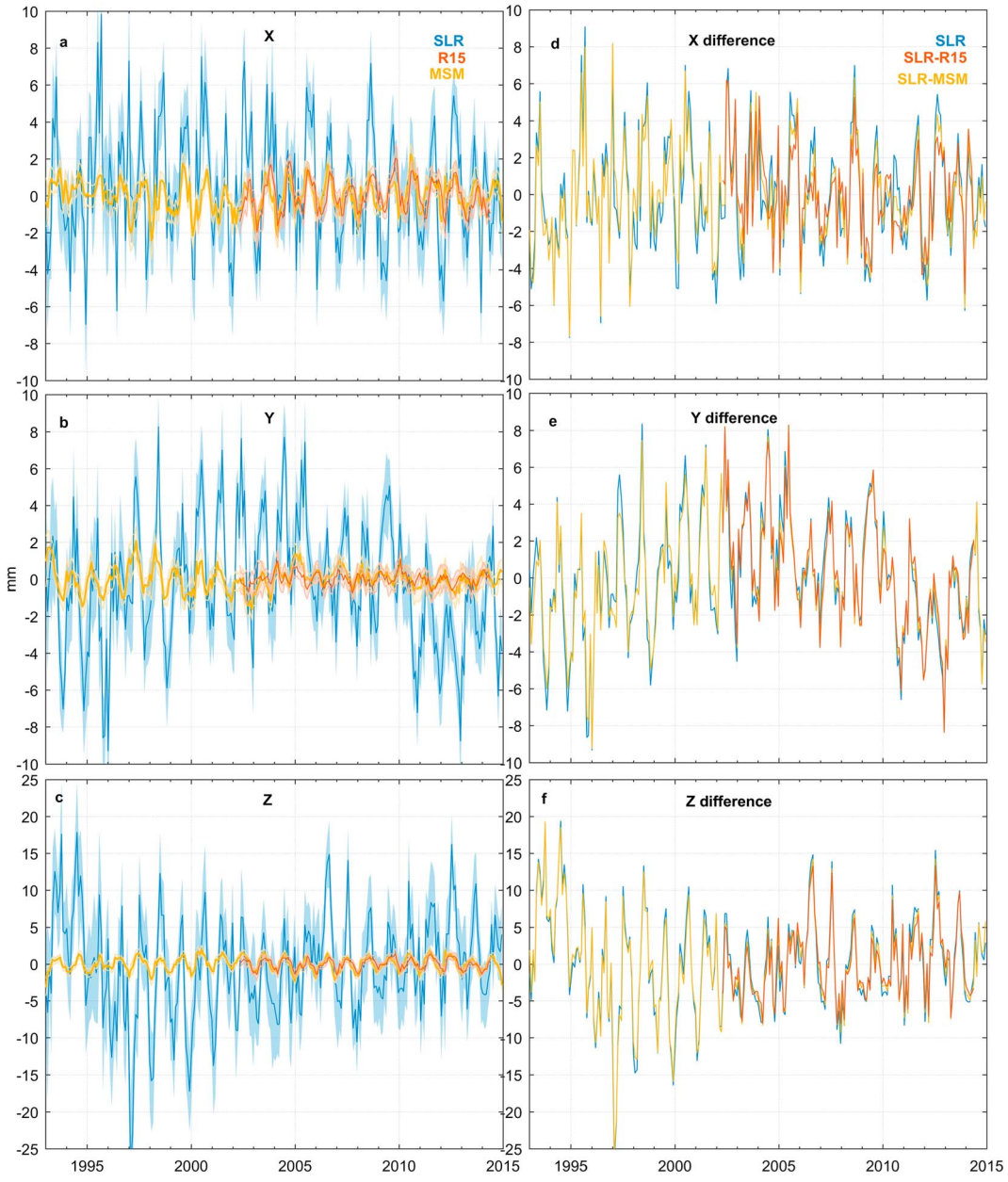

Figure 1. SLR translation components and two mass transport models (R15 and MSM). (a–c) Monthly translation series from SLR [1993.0–2015.0], R15 [2002.3–2014.5], and MSM [1993.0–2015.0] for each component (*X*, *Y*, and *Z*); the shaded area is transformation uncertainty. (d–f) SLR and differences of detrended monthly network translation time series for each component where the models have been subtracted from the SLR time series. Note the differences in scale of the *Z* component plots (Figures 1c and 1f) versus the *X* and *Y* components (Figures 1a, 1b, 1d, and 1e).

Figures 1d–1f show the SLR translations alongside the differences of R15 and MSM with SLR, where the qualitative agreement of the curves reveals that the differences are heavily influenced by signal not in R15 and MSM. Considering the residual series, the percentage of SLR variance explained by R15 is 12.5%, 1.3%, and 2.1% for the *X*, *Y*, and *Z* components, respectively, with MSM explaining 8.1%, 4.0%, and 2.0%, respectively. The small proportion of variance explained by the surface mass transport models indicates that either the geophysical models are not able to capture the surface mass transport variability or systematic errors from the SLR technique are substantial. The visual agreement between R15 and MSM is noteworthy given the dissimilarity in the data used to construct the series. Surface thermoelastic effects, with annual amplitudes

Journal of Geophysical Research: Solid Earth

10.1002/2016JB013698

Table 1. Noise Parameters From HECTOR of the Full SLR Data Set and MSM Network Translation Model [1993.0 2015.0][a]

	SLR			MSM			SLR-MSM		
Model	White-Only	PLW	GGM	White-Only	PLW	GGM	White-Only	PLW	GGM
				X					
AIC	1323.350	1282.103	1256.500	438.639	393.762	392.735	1225.414	1204.903	1198.35
BIC	1323.350	1289.263	1263.659	438.639	400.921	399.894	1225.414	1212.062	1205.51
k	0	−0.80	0.98 ± 0.30	0	−0.59	0.62 ± 0.30	0	−0.50	0.47 ± 0.18
1 phi			0.51 ± 0.14			0.02 ± 0.03			0.36 ± 0.19
STD	2.939	2.689	2.570	0.504	0.5041	0.554	2.443	2.3301	2.303
Bias (mm)	−0.000 ± 0.181	−0.197 ± 2.123	−0.014 ± 0.306	0.005 ± 0.034	0.042 ± 0.173	0.025 ± 0.098	0.001 ± 0.150	−0.102 ± 0.602	−0.003 ± 0.229
Trend (mm $yr^{-1)}$	−0.000 ± 0.028	0.017 ± 0.128	0.000 ± 0.048	−0.001 ± 0.005	−0.009 ± 0.016	−0.007 ± 0.014	−0.005 ± 0.024	0.007 ± 0.061	−0.003 ± 0.036
				Y					
AIC	1371.096	1222.215	1192.371	401.992	243.008	225.826	1193.983	1060.86	1064.138
BIC	1371.096	1229.374	1199.531	401.992	250.167	232.986	1193.983	1068.019	1071.297
k	0	−0.98	0.98 ± 0.13	0	−0.98	0.77 ± 0.11	0	−0.94	0.36 ± 0.04
1 phi			0.29 ± 0.08			0.17 ± 0.08			0.01 ± 0.01
STD	3.216	2.391	2.275	0.517	0.3769	0.367	2.302	1.7056	1.786
Bias (mm)	−0.000 ± 0.198	−0.451 ± 8.952	−0.024 ± 0.473	0.008 ± 0.032	0.085 ± 1.318	0.025 ± 0.088	0.001 ± 0.141	−0.374 ± 2.525	−0.218 ± 0.567
Trend (mm $yr^{-1)}$	0.000 ± 0.031	−0.027 ± 0.166	−0.008 ± 0.073	0.000 ± 0.005	−0.007 ± 0.026	−0.002 ± 0.013	0.006 ± 0.022	0.003 ± 0.082	0.002 ± 0.069
				Z					
AIC	1761.462	1638.007	1585.610	367.806	318.881	316.801	1626.136	1512.313	1508.971
BIC	1761.462	1645.166	1592.769	367.806	326.04	323.96	1626.136	1519.473	1516.13
k	0	−0.93	1.48 ± 0.32	0	−0.66	0.37 ± 0.07	0	−0.86	0.49 ± 0.07
1 phi			0.48 ± 0.10			0.05 ± 0.06			0.05 ± 0.04
STD	6.717	5.252	4.777	0.484	0.4375	0.436	5.203	4.1494	4.135
Bias (mm)	−0.000 ± 0.413	0.637 ± 9.503	0.017 ± 0.871	0.004 ± 0.030	−0.053 ± 0.191	−0.025 ± 0.078	0.010 ± 0.320	0.892 ± 4.456	0.284 ± 1.061
Trend (mm $yr^{-1)}$	−0.000 ± 0.065	−0.044 ± 0.328	0.006 ± 0.135	0.003 ± 0.005	0.004 ± 0.015	0.003 ± 0.012	−0.014 ± 0.05	−0.077 ± 0.223	−0.026 ± 0.156

[a]AIC is a measure of the relative quality of statistical models for a given set of data; BIC is a criterion for model selection among a finite set of models; the model with the lowest AIC/BIC value is preferred; *k* is the spectral index; 1 phi is a GGM parameter; STD is the standard deviation (units mm).

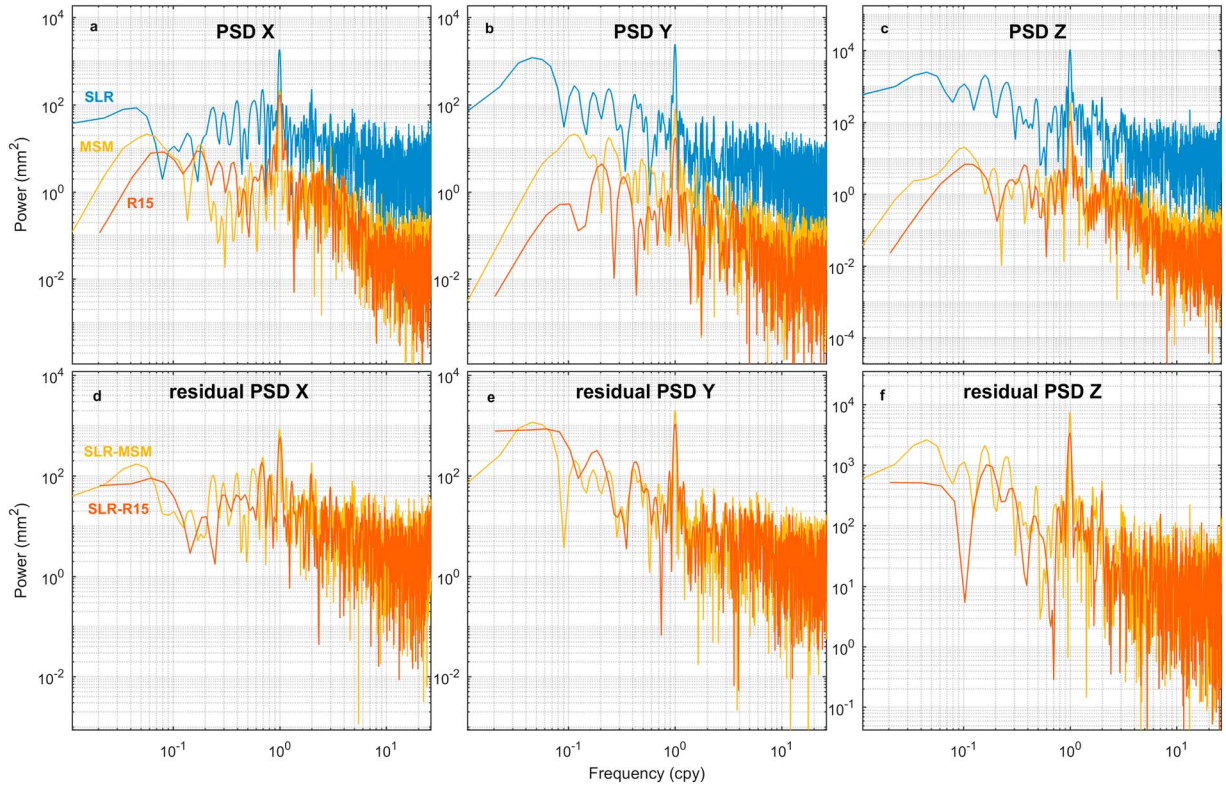

Figure 2. (a–c) PSD from Lomb-Scargle analysis of the data from SLR [1993.0–2015.0], R15 [2002.3–2014.5], and MSM [1993.0–2015.0], for each time series component (*X*, *Y*, and *Z*). (d–f) PSD of the residuals (data from Figures 1d–1f) for each component. Note the differences in scale of the *Z* component plots (Figures 2c and 2f) versus the *X* and *Y* components (Figures 2a, 2b, 2d, and 2e).

approaching 3 mm for radial displacements and 1.5 mm for transverse displacements [*Xu et al*., 2017], could explain some of the difference between the SLR translations and the respective network translations.

3.1. Seasonal Variation

The dominant signal throughout the SLR translation series has an annual period with apparent variable amplitude. Over the full time series, the SLR translation annual signal in the *Z* component is approximately twice that of the SLR translation *X* and *Y* components (see Table 1). The greatest agreement in overall amplitude and its temporal variation between SLR, R15, and MSM is found in the *X* component, which is predominantly ocean driven due to the limited land area along the *X* axis (*X* is in the direction of 0°N 0°E, *Y* of 0°N, and *Z* of 90°N).

The annual signal expressed in the residuals for each coordinate component (Figures 1d–1f, SLR minus model) computed between the SLR origin and model-based network translation estimates demonstrates reasonable qualitative agreement in phase and amplitude, again demonstrating that both the R15 and MSM models significantly underestimate the amplitude of the annual signal within the SLR translations. To explore the strength of the annual signals more closely, we computed the power spectral density (PSD) using the Lomb-Scargle approach described by *Press et al.* [1992]. Figure 2 shows the PSD for each data set across each coordinate component. Lower frequency trends are less well resolved by R15 due to the restricted temporal span, and care should be taken not to overinterpret differences at these frequencies.

The annual signal expressed in MSM significantly underestimates the observed SLR amplitude in all components, particularly during the latter part of the *Y* component time series (Figure 1b) and remains visible as a peak in the residual PSD (Figure 2e). The shorter duration R15 model also underestimates the magnitude of the annual signal, where the most notable differences for both R15 and MSM are with respect to the *Z* component (Figure 1c). This is confirmed by the presence of a residual peak at the 1 c/yr frequency in Figures 2d–2f.

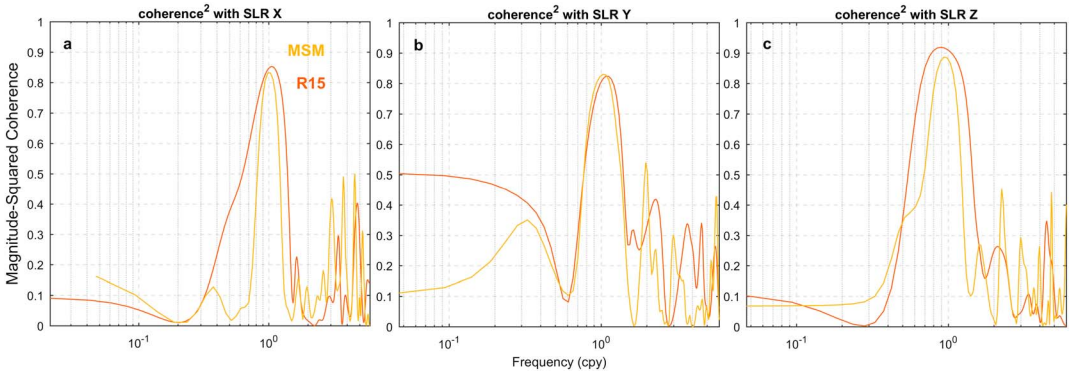

Figure 3. (a–c) Coherence-squared of SLR translation components with network translations from surface mass transport models (R15 and MSM).

The SLR series was compared with the MSM translations over the same time span as R15 (results not plotted here). In this analysis, the annual signal amplitude and phase of MSM were not statistically different from R15 in comparison to SLR over the shortened time span. The MSM data set, over the R15 time span, is very similar to the SLR *Y* component but has reduced agreement with the SLR *X* and *Z* components, particularly in the latter part (2002 onward) of the time series (similarly as for R15) where the signal deviates (Figure 1). That the surface mass transport models are indistinguishable from each other in the later part of the time series provides confidence in their construction, noting again the dissimilarities in their constituent data series.

The magnitude-squared coherence of the SLR time series with each of the models in Figure 3 provides further evidence that an annual signal is clearly present in both the observations from SLR and the network translation estimates from geophysical models. A strong peak in each component is centered about 1 c/yr, with an average magnitude-squared coherence of 0.9 across the *X*, *Y*, and *Z* components. Figure 3a shows that agreement in the *X* component is poor for signals other than annual, particularly between SLR and R15. Better agreement at other frequencies is evident in the *Y* and *Z* components between SLR and the network translation models. Other less significant peaks are observed at subannual periods, but they are not considered further here.

To assess the time variability of the time series, we follow a similar method to *Argus* [2012], whereby each time series is divided into 4 year segments, each overlapping by 1 year, producing seven segments in our analysis. A linear plus seasonal model was fitted to each segment, with the amplitude for each origin component shown in Figures 4a–4c, each centered on the midpoint of the segment. Four years is sufficient to reliably estimate the linear plus annual and semiannual terms [*Blewitt and Lavallée*, 2002]. For the SLR data, a number of annual amplitudes computed from segmented data are significantly different to those computed over the full series in the *Y* and *Z* components. While natural variation in these terms is expected, some of the behavior appears systematic and specific to SLR. For example, the *Y* component shows a marked reduction in amplitude following the segment centered on 2003.5 (Figure 4b), which is not reflected in the R15 data, and only marginally reflected in the MSM data. The largest variability in SLR annual amplitude is found in the *Z* component (Figure 4c), with the large deviation in the segment centered on 1997.5 not reproduced by either R15 or MSM.

We also note a decrease in the uncertainty of the annual amplitude across the SLR data segments, most noticeably in the *X* and *Z* components. This perhaps reflects refinements in the SLR observing networks' geometry and operation capacity over time [*Varghese,* 2013].

3.2. Noise Characteristics

Examination of Figure 2 shows clear features other than the dominant annual signals. The noise floor of the SLR data set is substantially higher than that of both the network translation models, presumably associated the effect of measurement error. The SLR *X* component (Figure 2a) shows a flatter (whiter) spectrum than in *Y* and *Z* indicating increased time-correlated noise in the latter components. The spectra of SLR-R15 and SLR-MSM (Figures 2d–2f) also suggest time-correlated noise across each component.

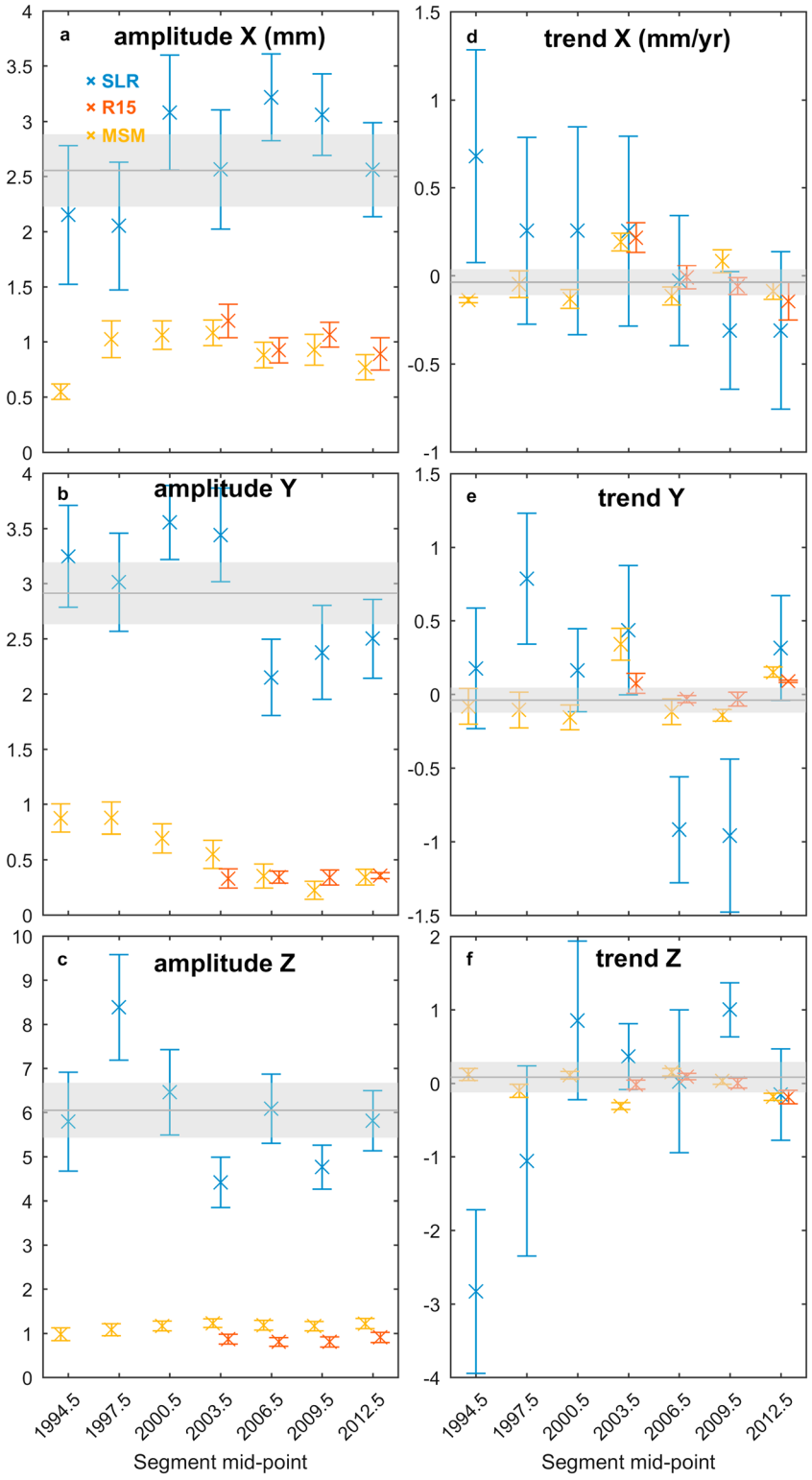

Figure 4. (a–c) Annual amplitude and uncertainty of each network translation component where each data set has been segmented into 4 year segments with 1 year overlap for SLR, R15, and MSM with a PLW noise model. Uncertainties are one sigma. (d–f) Linear rates and uncertainty with a PLW noise model of the time series (Figures 1d–1f). The shaded area is the respective amplitude and linear rate values for the full SLR time series with 1 sigma uncertainty [1993.0–2015.0]. R15 and MSM have been offset in time for clarity. Four year segments are as follows: 1993.0–1997.0, 1996.0–2000.0, 1999.0–2003.0, 2002.0–2006.0, 2005.0–2009.0, 2008.0–2012.0, and 2011.0–2015.0.

Journal of Geophysical Research: Solid Earth

10.1002/2016JB013698

Table 2. Noise Parameters From HECTOR of the Shortened SLR Data Set and R15 Network Translation Model [2002.3–2014.5]

	SLR			R15			SLR-R15		
Model	White-Only	PLW	GGM	White-Only	PLW	GGM	White-Only	PLW	GGM
				X					
AIC	717.384	688.717	668.043	205.392	182.117	171.120	635.281	627.398	623.919
BIC	717.384	694.698	674.024	205.392	188.084	177.087	635.281	633.365	629.886
k	0	−0.90	1.13 ± 0.39	0	−0.67		0	−0.47	0.44 ± 0.23
1 phi			0.50 ± 0.16						0.35 ± 0.26
STD	2.776	2.464	2.313	0.489	0.443	0.428	2.131	2.043	2.021
Bias (mm)	−0.000 ± 0.229	−0.008 ± 3.682	−0.022 ± 0.413	0.026 ± 0.040	−0.031 ± 0.225	0.022 ± 0.062	0.066 ± 0.176	0.183 ± 0.559	0.072 ± 0.265
Trend (mm $yr^{-1)}$	−0.000 ± 0.065	−0.014 ± 0.270	0.004 ± 0.115	0.009 ± 0.012	0.012 ± 0.032	0.009 ± 0.017	−0.101 ± 0.050	−0.105 ± 0.106	−0.104 ± 0.075
				Y					
AIC	705.882	646.078	628.424	−20.596	−43.518	−46.146	572.596	551.285	550.747
BIC	705.882	652.059	634.405	−20.596	−37.551	−40.178	572.596	557.252	556.514
k	0	−0.93	0.92 ± 0.19	0	−0.63	0.39 ± 0.11	0	−0.80	0.29 ± 0.07
1 phi			0.31 ± 0.11			0.12 ± 0.12			0.06 ± 0.06
STD	2.670	2.129	2.020	0.225	0.205	0.204	0.719	1.5286	1.573
Bias (mm)	0.000 ± 0.220	0.204 ± 3.932	0.043 ± 0.485	0.002 ± 0.190	−0.001 ± 0.091	0.003 ± 0.038	0.325 ± 0.142	0.357 ± 0.962	0.342 ± 0.291
Trend (mm $yr^{-1)}$	0.000 ± 0.062	0.079 ± 0.245	0.022 ± 0.133	−0.006 ± 0.005	−0.001 ± 0.014	−0.004 ± 0.010	−0.387 ± 0.041	−0.351 ± 0.109	−0.368 ± 0.078
				Z					
AIC	905.651	860.284	832.483	141.685	121.640	112.263	787.566	766.569	764.327
BIC	905.651	866.265	838.464	141.685	127.607	118.230	787.566	772.536	770.294
k	0	−0.95	1.33 ± 0.37	0	−0.63		0	−0.61	0.36 ± 0.10
1 phi			0.49 ± 0.13			0.99 ± 0.00			0.10 ± 0.11
STD	5.267	4.404	4.044	0.393	0.361	0.350	3.590	3.287	3.268
Bias (mm)	0.000 ± 0.434	−0.023 ± 10.493	0.006 ± 0.860	0.002 ± 0.033	−0.017 ± 0.157	0.003 ± 0.048	0.100 ± 0.297	−0.019 ± 1.337	0.052 ± 0.612
Trend (mm $yr^{-1)}$	−0.000 ± 0.123	−0.066 ± 0.529	0.032 ± 0.239	0.006 ± 0.009	−0.002 ± 0.024	0.006 ± 0.014	0.239 ± 0.085	0.197 ± 0.214	0.201 ± 0.167

To further examine the properties of the time-correlated noise, we tested various noise models for each data set using HECTOR software [*Bos et al*., 2013], examining white noise only, random walk, flicker, autoregressive moving average, autoregressive fractionally integrated moving average, generalized Gauss-Markov (GGM) or power law and white (PLW) models. Noise model parameters and summary statistics were estimated along with a linear rate and annual plus semiannual periodic terms. We used both the Akaike information criterion [*Akaike*, 1973] and Bayesian information criterion [*Schwarz*, 1978] to identify the preferred noise model for each time series. The characteristics of the SLR series are best fit by a GGM or PLW model, in strong preference to a white noise-only model (see Table 1). Where a white noise-only model was estimated in HECTOR, our values are consistent with the time-constant annual and semiannual terms of *Altamimi et al.* [2016].

The uncertainty in the rate of the SLR translations, estimated with a PLW noise model over the complete time span, is a factor of 5 larger in comparison to a white noise-only model (see Table 1). That is, white noise uncertainties for *X*, *Y*, and *Z* rates, respectively, of ±0.03, ±0.03, and ±0.06 increase to ±0.13, ±0.17, and ±0.33 (mm/yr) when a PLW noise model is adopted. A PLW noise model was chosen instead of GGM for the remaining analysis as a conservative estimate of rate uncertainty. We examined the apparent offset around 2010 in the SLR origin *Y* component (Figures 1b and 1e), as described by *Altamimi et al.* [2016], and found it to be statistically insignificant when estimated as an offset within the noise analysis. Neither of the geophysical models shows an offset at this time. Together, this suggests that the apparent discontinuity is simply characteristic of power law time-correlated noise with spectral indices close to −1 (flicker noise) [*Williams*, 2003]. No other offsets were estimated for the data sets.

Neither of the network translations from the geophysical models captures the long-period variability in the SLR series particularly well. The removal of the models from the SLR series results in generally no change to the spectral index for the PLW model in the *X*, *Y*, and *Z* components for both MSM and R15, (see Tables 1 and 2).

3.3. Time-Variable Trends

We next consider the multiyear trends in the SLR translation time series. By convention, the linear rate of each SLR origin translation component is not statistically different from zero [*Altamimi et al*., 2016] over the full time series. However, low-frequency variability is evident in the SLR time series, particularly in the *Y* and *Z* components (Figures 1b and 1c). This signal is not present in either of the mass transport models (Figure 1, noting that the same scale is used in the left and right panels). The nonlinear signature observed in the temporal domain of the SLR *Y* component in Figure 1b is similarly reflected in Figure 2b where the *Y* component of the SLR origin series shows high power at low frequencies.

The time-variable rate within each data series is shown in Figures 4d–4f, for each of the 4 year segments discussed previously. Similarly to the annual amplitude, the largest temporal variability in the short-term rate is found in the SLR *Y* and *Z* components (Figures 4e and 4f), with a number of short-term rates significantly different to the rate determined over the full record (grey line, Figures 4d–4f). The section of the SLR *X* and *Z* components before 1997.0 are distinctly different from the long-term average, with the *Z* component almost a factor of 3 larger than the long-term mean in this period. Segments in the *Y* component have differences from the mean ranging from +0.8 mm/yr to −0.9 mm/yr, and the two segments covering 2005.0–2012.0 are statistically significant from the long-term average. R15 contains contributions from ocean mass and ice sheets mass that are indirectly affected by the GIA model used, which are not included in MSM and could explain some of the offset between the rates derived from the two models.

4. Discussion

Our comparison of the SLR translations with respect to the ITRF2014 origin with network translations derived from equivalently sampled geophysical models shows that it is likely that signals of nongeophysical origin, with a range of frequencies (monthly to interannual), are insufficiently accounted for in the stochastic model of the ITRF2014 origin. *Altamimi et al.* [2016] suggested to add annual corrections to the station positions (equations (2) and (3) in their paper) in order to bring the network origin closer to the instantaneous CM, as sensed by SLR. However, if the annual estimates are partly affected by systematic errors in SLR, it remains unclear how these errors will propagate into station positions (and satellite orbits) if the published annual and semiannual geocenter terms derived from SLR are applied.

Several studies have examined potential systematic error in SLR, in particular, the influence of the time-variable ground network distribution [*Collilieux et al*., 2009; *Collilieux and Wöppelmann*, 2011], and satellite observation geometry [*Spatar et al*., 2015] in order to assess uncertainty. *Collilieux et al.* [2009] found that the SLR network effect could affect the amplitude of the annual geocenter motion in the *Z* direction at approximately 1 mm, depending on the simulated observing network geometry. We found that the network effect was dominated by the geophysical models' annual signal, rather than the network geometry and account for the SLR network effect by deriving network translations from geophysical models, using only the surface deformation at those active SLR stations for each epoch.

Previous studies have explored uncertainty in the data series submitted to the previous ITRF, ITRF2008 [*Altamimi et al*., 2011], and found substantial nonlinear variation around the origin [*Métivier et al*., 2010; *Argus*, 2012]. *Dong et al.* [2014] note an acceleration in the *Z* geocenter component of the ITRF2008 origin after 1998 and attribute this to terrestrial water mass redistribution, including mass loss from continental ice sheets and glaciers. We note the same feature in our analysis with a clear change in the short-term rate of the SLR *Z* component (Figure 4f), but note that this is not replicated by MSM, even though MSM and *Dong et al.* [2014] both use the GLDAS terrestrial water storage model. We note that there are differences in the glacier and ice sheet mass terms which could explain why the deviation is not present in MSM; the reason for this discrepancy requires further consideration.

Both the land glacier and dam retention components of the MSM surface mass transport model have insufficient temporal resolution to capture the annual component of these constituents. The resolution of surface displacements due to terrestrial water storage changes remains challenging due to deficiencies in hydrologic models, in particular, the long-term trends and accurate representation of groundwater use. The missing annual hydrologic signal could explain some of the gap between SLR and MSM, but we note that this signal is included in R15 which also does not agree with SLR in amplitude over a short period.

Others have evaluated the stability of the ITRF2008 origin using statistical and spectral analysis [*Collilieux and Altamimi*, 2013; *Argus*, 2012]. These analyses show that a colored noise model is more appropriate than a white noise-only model; an outcome that we find remains robust for the ITRF2014 origin. *Argus* [2012] demonstrated time variability in both the annual amplitude and short-term rates of geocenter motion and that the linear CM velocity uncertainties are ±0.4 mm/yr for *X* and *Y* and ±0.9 mm/yr for the *Z* component (95% confidence limit). Our findings confirm that a simple linear regression using a white noise-only model will poorly reflect the true uncertainty of the estimated parameters, with the uncertainty for the linear rate typically a factor of 5 smaller than estimates using a PLW noise model (see Tables 1 and 2). Our analysis of the SLR translations relative to the ITRF2014 origin suggests improvement of the CM velocity compared with those from *Argus* [2012] for ITRF2008. Simply scaling our rate uncertainties to 2 sigma, the PLW noise model results in a 27% improvement of the SLR *Z* component, reducing from ±0.9 mm/yr (95% confidence limit) [*Argus*, 2012] to ±0.66 mm/yr (95% confidence limit).

The future improvement of the precision and accuracy of the ITRF origin will depend on advances in analysis of SLR data and improved network geometry. Indeed, the present SLR station geometry is suboptimal, with a concentration of SLR stations in the Northern Hemisphere decreasing the precision of the *Z* component compared to the equatorial components [*Bouillé et al*., 2000*; Collilieux and Wöppelmann*, 2011; *Wu et al*., 2012]. *Otsubo et al.* [2016] confirmed this finding with a simulation study indicating that the addition of a station at low latitudes (15°S–30°S) would improve the precision of the *Z* component of the geocenter and that additional sites at high latitudes, particularly in the south, would provide an important improvement in the *X* and *Y* geocenter components.

5. Conclusions

We assess the temporal variability of the latest SLR translations with respect to the International Terrestrial Reference Frame (ITRF2014) origin and find significant differences when compared to modeled network translations from two independent surface mass transport models. The proportion of variance explained in the SLR origin time series by geophysical models is on average less than 10% in each component. We identified colored noise in both observed and modeled network translation time series, but substantial colored noise remains after subtraction of the model based translations, with notable signal remaining at annual and longer periods. Consideration of power law noise when estimating the rate in the origin components

yields an upper bound fivefold increase in rate uncertainty, compared to the white noise-only case. When using a power law and white model, the uncertainty of the SLR *Z* component (0.33 mm/yr; 1 sigma) is twice as large as that of the *X* and *Y* components (0.13 and 0.17 mm/yr, respectively). This represents a 27% improvement for the *Z* component of the results in comparison to those from *Argus* [2012] for ITRF2008.

Over shorter time periods, the temporal variability of linear rates computed over 4 years suggests that the SLR translations with respect to the long-term ITRF2014 origin cannot be rigorously represented by a simple linear model over longer periods. For the annual signal, model-based network translations, particularly in the *Z* component, do not represent the variability in the annual amplitude of the SLR translations with respect to the ITRF2014 origin. This indicates that a significant component of the signal is due to other processes, including likely large systematic error.

Positioning uncertainty for geophysical applications is likely to be impacted by nonlinear geophysical signals of the kind we identify in the SLR translation time series with respect to the ITRF2014 origin and may be further impacted when nongeophysical signals exist. Space geodetic analyses that require an instantaneous CM frame (precise orbit determination, for example) will also likely be affected given that the annual geocenter motion model used is derived from the same SLR data that are used to define the long-term origin of ITRF2014. Further improvements in SLR data analysis and network geometry are likely required to address this issue. The demonstration of other geodetic techniques to contribute to the Earth's center of mass determination would also be of great benefit.

Acknowledgments

A.R.R. is a recipient of scholarship funding from Geoscience Australia. M.A.K. is a recipient of an Australian Research Council Future Fellowship (project FT110100207). R.E.M.R. acknowledges funding by the Netherlands Organisation for Scientific Research (NWO) through VIDI grant 864.12.012. Y.S. acknowledges funding from Chinese Scholarship Council (CSC). This work was partially supported by the Australia-Germany Joint Research Cooperation Scheme. We thank Zuheir Altamimi for the provision of the SLR translation data. Ben Marzeion, Michiel van den Broeke, and Yoshi Wada are thanked for data sharing. The HECTOR software is freely available (http://segal.ubi.pt/hector/). We thank Paul Tregoning, Zuheir Altamimi, and a further anonymous reviewer for their comments which contributed to improving the quality and clarity of the manuscript.

References

Akaike, H. (1973), Information theory and an extension of the maximum likelihood principle, in *Second International Symposium on Information Theory*, edited by B. N. Petrov and B. F. Csaki, pp. 267–281, Academiai Kiado, Budapest.

Altamimi, Z., X. Collilieux, J. Legrand, B. Garayt, and C. Boucher (2007), ITRF2005: A new release of the International Terrestrial Reference Frame based on time series of station positions and Earth orientation parameters, *J. Geophys. Res.*, *112*, B09401, doi:10.1029/2007JB004949.

Altamimi, Z., X. Collilieux, and L. Métivier (2011), ITRF2008: An improved solution of the International Terrestrial Reference Frame, *J. Geod.*, *85*(8), 457–473, doi:10.1007/s00190-011-0444-4.

Altamimi, Z., P. Rebischung, L. Métivier, and X. Collilieux (2016), ITRF2014: A new release of the International Terrestrial Reference Frame modeling non-linear station motions, *J. Geophys. Res. Solid Earth*, *121*, 6109–6131, doi:10.1002/2016JB013098.

Appleby, G., J. Rodríguez, and Z. Altamimi (2016), Assessment of the accuracy of global geodetic satellite laser ranging observations and estimated impact on ITRF scale: Estimation of systematic errors in LAGEOS observations 1993–2014, *J. Geod.*, *1–18*, 1371–1388, doi:10.1007/s00190-016-0929-2.

Argus, D. F. (2012), Uncertainty in the velocity between the mass center and surface of Earth, *J. Geophys. Res.*, *117*(B10), 1–15, doi:10.1029/2012JB009196.

Blewitt, G. (2003), Self-consistency in reference frames, geocenter definition, and surface loading of the solid Earth, *J. Geophys Res.*, *108*(B2), 2103, doi:10.1029/2002JB002082.

Blewitt, G., and D. Lavallée (2002), Effect of annual signals on geodetic velocity, *J. Geophys. Res.*, *107*(B7), 2145, doi:10.1029/2001JB000570.

Bos, M. S., R. M. S. Fernandes, S. D. P. Williams, and L. Bastos (2013), Fast error analysis of continuous GNSS observations with missing data, *J. Geod.*, *87*(4), 351–360, doi:10.1007/s00190-012-0605-0.

Bouillé, F., A. Cazenave, J. M. Lemoine, and J. F. Crétaux (2000), Geocentre motion from the DORIS space system and laser data to the LAGEOS satellites: Comparison with surface loading data, *Geophys. J. Int.*, *143*(1), 71–82, doi:10.1046/j.1365-246x.2000.00196.x.

Chao, B. F., Y. H. Wu, and Y. S. Li (2008), Impact of artificial Reservoir water impoundment on global sea level, *Science*, *320*(5873), 212–214, doi:10.1126/science.1154580.

Collilieux, X., and Z. Altamimi (2013), External Evaluation of the origin and scale of the International Terrestrial Reference Frame, in *Reference Frames for Applications in Geosciences*, edited by Z. Altamimi and X. Collilieux, pp. 27–31, Springer, Berlin, doi:10.1007/978-3-642-32998-2_5.

Collilieux, X., and G. Wöppelmann (2011), Global sea-level rise and its relation to the terrestrial reference frame, *J. Geod.*, *85*(1), 9–22, doi:10.1007/s00190-010-0412-4.

Collilieux, X., Z. Altamimi, J. Ray, T. van Dam, and X. Wu (2009), Effect of the satellite laser ranging network distribution on geocenter motion estimation, *J. Geophys. Res.*, *114*, B04402, doi:10.1029/2008JB005727.

Collilieux, X., T. van Dam, J. Ray, D. Coulot, L. Métivier, and Z. Altamimi (2012), Strategies to mitigate aliasing of loading signals while estimating GPS frame parameters, *J. Geod.*, *86*(1), 1–14, doi:10.1007/s00190-011-0487-6.

Dong, D., J. O. Dickey, Y. Chao, and M. K. Cheng (1997), Geocenter variations caused by atmosphere, ocean and surface ground water, *Geophys. Res. Lett.*, *24*(15), 1867–1870, doi:10.1029/97GL01849.

Dong, D., W. Qu, P. Fang, and D. Peng (2014), Non-linearity of geocentre motion and its impact on the origin of the terrestrial reference frame, *Geophys. J. Int.*, *198*(2), 1071–1080, doi:10.1093/gji/ggu187.

Dong, D., T. Yunck, and M. Heflin (2003), Origin of the International Terrestrial Reference Frame, *J. Geophys. Res.*, *108*(B4), 2200, doi:10.1029/2002JB002035.

Dziewonski, A. M., and D. L. Anderson (1981), Preliminary reference Earth model, *Phys. Earth Planet. Inter.*, *25*(4), 297–356, doi:10.1016/0031-9201(81)90046-7.

Farrell, W. E. (1972), Deformation of the Earth by surface loads, *Rev. Geophys.*, *10*(3), 761–797, doi:10.1029/RG010i003p00761.

Flechtner, F., H. Dobslaw, and E. Fagiolini (2015), AOD1B product description document for product release 05 (Rev. 4.3), Tech. Rep., GFZ German Research Center for Geosciences, Postdam.

Frederikse, T., R. Riva, M. Kleinherenbrink, Y. Wada, M. van den Broeke, and B. Marzeion (2016), Closing the sea level budget on a regional scale: Trends and variability on the northwestern European continental shelf, *Geophys. Res. Lett.*, *43*, 10,864–10,872, doi:10.1002/2016GL070750.

Gordeev, R. G., B. A. Kagan, and E. V. Polyakov (1977), The effects of loading and self-attraction on global ocean tides: The model and the results of a numerical experiment, *J. Phys. Oceanogr.*, *7*(2), 161–170, doi:10.1175/1520-0485(1977)007<0161:TEOLAS>2.0.CO;2.

Gross, R., G. Beutler, and H.-P. Plag (2009), Integrated scientific and societal user requirements and functional specifications for the GGOS, in *Global Geodetic Observing System: Meeting the Requirements of a Global Society on a Changing Planet in 2020*, edited by H.-P. Plag and M. Pearlman, pp. 209–224, Springer Berlin, doi:10.1007/978-3-642-02687-4_7.

Herring, T., M. A. Floyd, R. W. King, and S. McClusky (2015), Globk reference manual, global Kalman filter VLBI and GPS analysis program, release 10.6, Massachusetts Institute of Technology.

Lehner, B., et al. (2011), High-resolution mapping of the world's reservoirs and dams for sustainable river-flow management, *Front. Ecol. Environ.*, *9*(9), 494–502, doi:10.1890/100125.

Marzeion, B., P. W. Leclercq, J. G. Cogley, and A. H. Jarosch (2015), Brief communication: Global reconstructions of glacier mass change during the 20th century are consistent, *Cryosphere*, *9*, 2399–2404, doi:10.5194/tc-9-2399-2015.

Métivier, L., M. Greff-Lefftz, and Z. Altamimi (2010), On secular geocenter motion: The impact of climate changes, *Earth Planet. Sci. Lett.*, *296*(3–4), 360–366, doi:10.1016/j.epsl.2010.05.021.

Mitrovica, J. X., M. E. Tamisiea, J. L. Davis, and G. A. Milne (2001), Recent mass balance of polar ice sheets inferred from patterns of global sea-level change, *Nature*, *409*(6823), 1026–1029. [Available at http://www.nature.com/nature/journal/v409/n6823/suppinfo/4091026a0_S1.html.]

Noël, B., W. J. van de Berg, E. van Meijgaard, P. Kuipers Munneke, R. S. W. van de Wal, and M. R. van den Broeke (2015), Evaluation of the updated regional climate model RACMO2.3: Summer snowfall impact on the Greenland ice sheet, *Cryosphere*, *9*(5), 1831–1844, doi:10.5194/tc-9-1831-2015.

Otsubo, T., K. Matsuo, Y. Aoyama, K. Yamamoto, T. Hobiger, T. Kubo-oka, and M. Sekido (2016), Effective expansion of satellite laser ranging network to improve global geodetic parameters, *Earth Planets Space*, *68*(1), 1–7, doi:10.1186/s40623-016-0447-8.

Press, W. H., S. A. Teukolsky, W. T. Vetterling, and B. P. Flannery (1992), *Numerical Recipes in C: The Art of Scientific Computing*, 2nd ed., pp. 575–584, Cambridge Univ. Press, Cambridge, U. K.

Rietbroek, R., S.-E. Brunnabend, J. Kusche, J. Schröter, and C. Dahle (2015), Global and regional sea level budget components from GRACE and radar altimetry (2002–2014), doi:10.1594/PANGAEA.855539, in supplement to: Rietbroek, Roelof; Brunnabend, Sandra-Ester; Kusche, Jürgen; Schröter, Jens; Dahle, Christoph (2016): Revisiting the contemporary sea level budget on global and regional scales, *Proc. Natl. Acad. Sci. U.S.A.*, *113*, 1504–1509, doi:10.1073/pnas.1519132113.

Rietbroek, R., S.-E. Brunnabend, J. Kusche, J. Schröter, and C. Dahle (2016), Revisiting the contemporary sea-level budget on global and regional scales, *Proc. Natl. Acad. Sci. U.S.A.*, *113*(6), 1504–1509, doi:10.1073/pnas.1519132113.

Rodell, M., et al. (2004), The Global Land Data Assimilation System, *Bull. Am. Meteorol. Soc.*, *85*(3), 381–394, doi:10.1175/BAMS-85-3-381.

Schwarz, G. (1978), Estimating the dimension of a model, *Ann. Stat.*, *6*(2), 461–464, doi:10.1214/aos/1176344136.

Spatar, C. B., P. Moore, and P. J. Clarke (2015), Collinearity assessment of geocentre coordinates derived from multi-satellite SLR data, *J. Geod.*, *89*(12), 1197–1216, doi:10.1007/s00190-015-0845-x.

Tamisiea, M. E., E. M. Hill, R. M. Ponte, J. L. Davis, I. Velicogna, and N. T. Vinogradova (2010), Impact of self-attraction and loading on the annual cycle in sea level, *J. Geophys. Res.*, *115*, C07004, doi:10.1029/2009JC005687.

van den Broeke, M. R., E. M. Enderlin, I. M. Howat, P. Kuipers Munneke, B. P. Y. Noël, W. J. van de Berg, E. van Meijgaard, and B. Wouters (2016), On the recent contribution of the Greenland ice sheet to sea level change, *Cryosphere*, *10*(5), 1933–1946, doi:10.5194/tc-10-1933-2016.

Varghese, T. (2013), Engineering changes to the NASA SLR network to overcome obsoleteness, improve performance and reliability, paper presented at Eighteenth International Workshop on Laser Ranging Instrumentation, Fujiyoshida, Japan.

Wada, Y., L. P. H. van Beek, C. M. van Kempen, J. W. T. M. Reckman, S. Vasak, and M. F. P. Bierkens (2010), Global depletion of groundwater resources, *Geophys. Res. Lett.*, *37*, L20402, doi:10.1029/2010GL044571.

Williams, S. D. P. (2003), Offsets in Global Positioning System time series, *J. Geophys. Res.*, *108*(B6), 2310, doi:10.1029/2002JB002156.

Wu, X., X. Collilieux, Z. Altamimi, B. L. A. Vermeersen, R. S. Gross, and I. Fukumori (2011), Accuracy of the International Terrestrial Reference Frame origin and Earth expansion, *Geophys. Res. Lett.*, *38*, L13304, doi:10.1029/2011GL047450.

Wu, X., J. Ray, and T. van Dam (2012), Geocenter motion and its geodetic and geophysical implications, *J. Geodyn.*, *58*, 44–61, doi:10.1016/j.jog.2012.01.007.

Xu, X., D. Dong, M. Fang, Y. Zhou, N. Wei, and F. Zhou (2017), Contributions of thermoelastic deformation to seasonal variations in GPS station position, *GPS Solutions*, 1–10, doi:10.1007/s10291-017-0609-6.